





Muon energy reconstruction in the high-energy neutrino observations

Ying Qi^{1,2,3,4}, Jiali Liu^{3,4*}, Maoyuan Liu^{1,2*} , Mingjun Chen^{3,4} , Zike Wang^{3,4,5} ,
Tianqi Huang^{3,4} , Peiyuan Chu^{3,4,5}

¹College of Science, Tibet University, Lhasa 850000, China

²Key Laboratory of Cosmic Rays, Ministry of Education, Tibet University, Lhasa 850000, China

³Institute of High Energy Physics, Chinese Academy of Sciences, Beijing 100049, China

⁴Tianfu Cosmic Ray Research Center, Chengdu 610000, China

⁵University of Chinese Academy of Sciences, Beijing 100049, China

*Correspondences: jliliu@ihep.ac.cn; liumaoyuan@163.com

Received: March 26, 2024; Accepted: April 11, 2024; Published Online: April 26, 2024; <https://doi.org/10.61977/ati2024027>

© 2024 Editorial Office of Astronomical Techniques and Instruments, Yunnan Observatories, Chinese Academy of Sciences. This is an open access article under the CC BY 4.0 license (<http://creativecommons.org/licenses/by/4.0/>)

Citation: Qi, Y., Liu, J. L., Liu, M. Y., et al. 2024. Muon energy reconstruction in the high-energy neutrino observations. *Astronomical Techniques and Instruments*, **1**(3): 197–202. <https://doi.org/10.61977/ati2024027>.

Abstract: The reconstruction of muon energies is crucial for the data analysis of neutrino experiments using large water Cherenkov detectors, but the resolution for muon energy reconstruction using traditional methods is poor. Here, we propose a revised approach to remove noisy optical modules along the track produced by the propagation of muons through water. The number of photons on the optical modules is first corrected by the attenuation properties of light in water. Then the difference in time between the observed optical modules and the expected ones is determined based on the geometry of the triggered optical modules. Finally, the standard of correction is measured by the ratio of photon number before and after correction. Optical modules selection conditions were optimized according to these parameters, with most noisy optical modules successfully removed, improving the resolution of muon energy reconstruction.

Keywords: dE/dx detectors; Neutrino detectors; Data processing

1. INTRODUCTION

Cosmic rays are high-energy particles originating from extraterrestrial sources, with energies ranging from ~ 10 GeV to $\sim 10^{11}$ GeV. High-energy neutrinos are generally considered to be produced by the inelastic collisions of high-energy cosmic rays with the cosmic baryon and photon background, known as hadronuclear and photo-hadronic interactions, respectively. Inelastic collisions can produce a variety of secondary particles, and the decay of these secondary particles generates high-energy neutrinos and gamma-ray photons. The numerical ratios of the six types of neutrinos produced by different reaction mechanisms vary. Neutrinos are electrically neutral and only interact weakly with matter. So they can travel through the universe undeflected by magnetic fields, making them almost perfect messengers for seeking the extragalactic origins of cosmic rays^[1].

The triumph of experiments such as IceCube and Baikal-GVD has proven that extended photodetector arrays, positioned either subaquatically or subglacially, are a cost-effective and efficient way of detecting high-energy

neutrinos. The Huge Underwater high-energy Neutrino Telescope (HUNT) is to be deployed under the sea with an effective volume of over 30 cubic kilometers. This initiative builds on the considerable scientific successes of the Large High Altitude Air Shower Observatory (LHAASO) in monitoring a variety of ultra-high energy PeV gamma sources. Aiming to make sensitive observations of a single neutrino source surpassing 50 TeV, the estimated angular resolution is $\sim 0.1^\circ$ (tracks) and 3° (cascades). Possible sites proposed for the project will be in the South China Sea or Lake Baikal in Russia^[2].

The basic design scheme of HUNT developed in this project, under the requirements mentioned above, comprises 2 304 strings spanning an area of $6 \text{ km} \times 6 \text{ km}$, arranged with 24 optical modules (OMs) on each string. The OM spacing within each string is 36 m, and the distance between the strings is 130 m (taking the Baikal station site as an example), i.e., a detector volume of 30 cubic kilometers is achieved (Fig. 1A). Observations are made with 20-inch upward-facing photomultiplier tubes (PMTs), used for the OMs (Fig. 1B), measuring the inten-

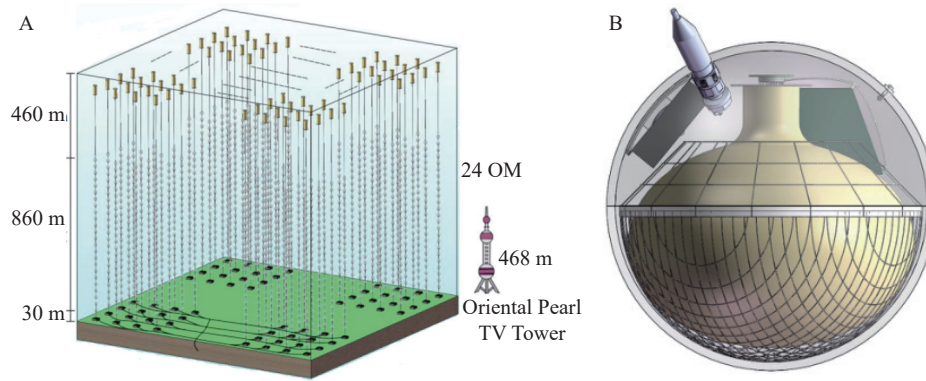


Fig. 1. A: A schematic diagram of the HUNT array^[2]. B: Illustration of an optical module, with a 20-inch PMT encapsulated inside a 23-inch glass sphere^[2].

sity and time information of the light signal. Each OM integrates LED scaled light sources, high-voltage modules, low-voltage power supplies, readout electronics, a thermohydrometer, and other equipment. All OMs are time-synchronized at the 1 ns level using the White Rabbit clock distribution system, and readouts are stored with 500 MHz waveform sampling. A sonar positioning system will be incorporated into the detector to monitor the position of all strings in real time to achieve better than 20 cm accuracy. Both LED and laser light sources are used to achieve time-relative difference scaling for all probes to achieve an accuracy of less than 1 ns. Waveforms are digitized in the OMs, and optical fibers transmit the data to the upper base station, and eventually the shore-based data acquisition system and computer center.

Muon neutrinos are produced by the ν_μ and ν_τ interactions. Muons have long tracks in the detector and a clear trajectory, and track events can be used to reconstruct their energies. The energy of muons is usually determined by measuring their energy loss on the way through the detector. Cherenkov photons produced by the muons, with photons produced by charged particles from random hadron interactions, are then counted during the measurement^[3]. Here, we propose a revised approach to remove OMs producing excessive noise (hereafter referred to as noisy OMs) along the track produced by the propagation of muons through the water. First, the number of photons detected by the OMs is corrected by the attenuation properties of light in water, and then the difference in time between the observed OMs and the expected OMs is determined based on the geometry of the triggered OMs. Finally, the standard of correction is measured by the ratio of the photon number before and after correction. The screening condition of OMs is optimized according to these parameters, removing the most noisy OMs and thereby improving the resolution of muon energy reconstruction.

The design scheme of the HUNT project offers significant advantages for the observation of muon events. First, the large detector volume and high-density array of OMs provide ample data for the detection and recording of muon events. The excellent angular and temporal resolu-

tion then enables precise measurement of the muon track and temporal features of interaction events.

This article covers all examples of muon track events generated in the detector. Section 2 describes how simulated events are generated, and Section 3 presents related concepts such as energy reconstruction, including signal correction, OM selection, photon density calculation and results. Section 4 presents the conclusions.

2. SIMULATION

We employ the GEANT4 software tool, developed by the European Organization for Nuclear Research (CERN), to perform multiple full simulations for HUNT experiment. This robust tool specializes in the simulation of particle transport through matter and includes a comprehensive set of features, including particle tracking, geometry modeling, physical models, and recording of detector responses (termed hits). During the simulation process, the G4ParticleGun is utilized to generate particles of specific types and energies. These particles are emitted from a predetermined source location and traverse a carefully designed detector geometry^[4]. GEANT4 meticulously logs the entirety of the particle transport data, allowing subsequent analysis of the energy reconstruction of the events. Fig. 2 illustrates an example of 100 TeV events generated by GEANT4. In the 100 TeV to 600 TeV energy range, 2 000 simulated events are generated at each energy at intervals of 100 TeV, giving 6 data samples in total. The simulated events are analyzed and processed, retaining the relevant data for energy reconstruction. Subsequently, each data sample is divided into two groups, with one contributing to the formulation of the energy reconstruction curve, while the other applies the derived curve to perform energy reconstruction.

3. ENERGY RECONSTRUCTION

Muons lose energy during propagation from ionization and stochastic processes, including pair production, bremsstrahlung emission, and photonuclear interactions^[3, 5]. The ionization process is independent of the muon

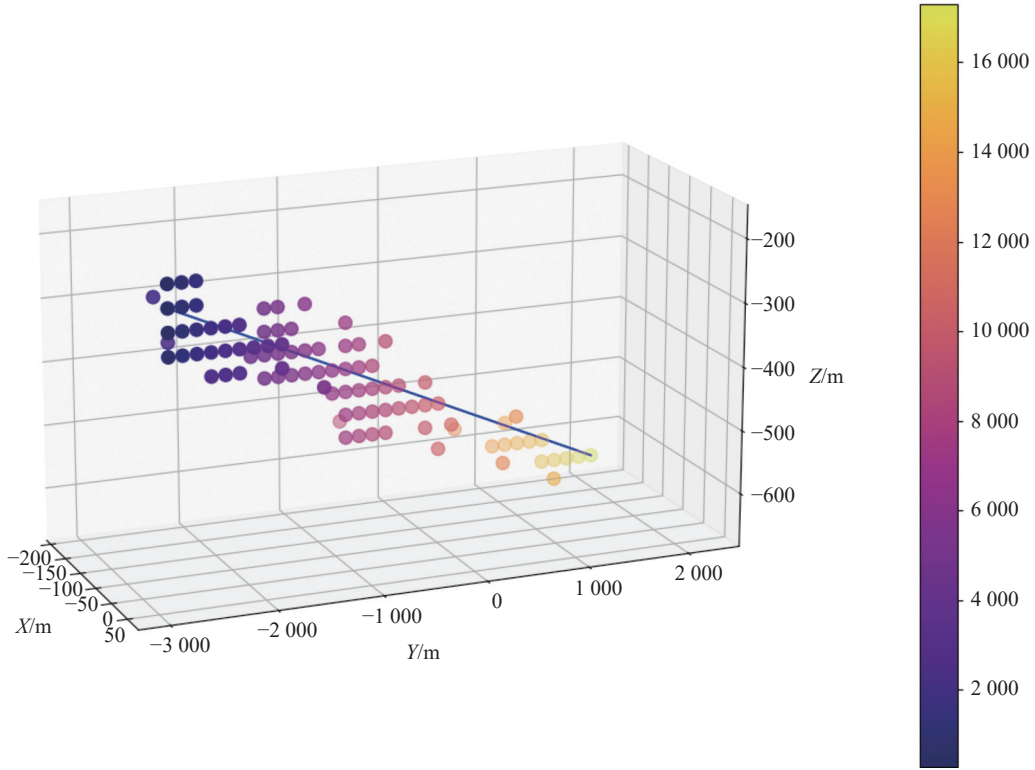


Fig. 2. A typical simulated muon. The color bar shows time in nanoseconds, x , y , and z axes are the locations of OMs measured in meters, and the blue line is the neutrino track, traveling from top left to bottom right.

energy, with the energy loss per unit length remaining essentially constant. However, the stochastic processes are energy-dependent and have a linear relationship to the muon energy. These stochastic processes become dominant when the muon energy exceeds 1 TeV^[6]. The average energy loss of a muon^[3] can be expressed as

$$\frac{dE_\mu}{dx} = -A - BE_\mu, \quad (1)$$

where A is the energy loss due to ionization and B is the energy loss due to stochastic processes.

When a muon passes through the detector array, it emits Cherenkov photons, which are detected as photoelectrons when the OM is illuminated. Muon energy reconstruction can be achieved by calculating the linear density of photons along different segments of the track.

Here, the energy reconstruction method is accomplished through a series of processes, including signal correction, selection of the OM, and calculation of photon density.

3.1. Signal Correction

Cherenkov photons produced along the muon trajectory travel through the water to the OMs, with distances depending on the location of photon generation and the OM. It is therefore necessary to correct the signals to avoid the influence of water attenuation on the photons. The number of photons is corrected using the formula

$$N_0 = N_e^{\frac{d}{\lambda}}, \quad (2)$$

where N_0 represents the number of photons after correction, N_e represents the number of photons detected by the OM, and d represents the distance from the OM to the track, corrected according to the Cherenkov angle. λ denotes the attenuation length of water (e.g. in Lake Baikal, Russia, $\lambda=18$ m)^[7]. This process can approximately revert the number of photons lost during propagation.

3.2. OM Selection

Once an event is generated via GEANT4, not all OMs collected in the event can participate in the reconstruction. To guarantee the accuracy, we need to remove the noisy OMs during the event. Fig. 3 shows a schematic representation of the photon propagation process along the muon trajectory. In it, point C , shown in orange, indicates where the muon enters the detector array, with the orange line showing the muon trajectory and the arrow giving the propagation direction of the muon. The Cherenkov photon is generated at point B , and point A , shown in red, indicates the OM which detects the photon.

We employ the time difference method to filter the desired OMs during an event. As shown in Fig. 3, there are four distinct temporal measurements: the average arrival time of photons at various emission angles on the OM, denoted as t_1 ($t_1 = t_{CB+BA}$); a reference time along the muon trajectory and one right-angled side of the triangle, denoted as t_2 ($t_2 = t_{CO+OA}$); the expected time for photons propagating to the OMs, assumed according to the Cherenkov emission angle ($\sim 42^\circ$), denoted as

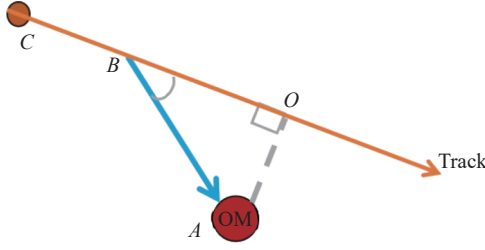


Fig. 3. Schematic diagram showing the generation of muons and the emission of photons toward the OM.

$t_1'(t_1' = t_{BA})$; and the time corresponding to the two right-angled sides of the triangle, denoted as $t_2'(t_2' = t_{BO+OA})$, where

$$\Delta t_1 = t_1 - t_2,$$

$$\Delta t_2 = t_1' - t_2', \quad (3)$$

and

$$\Delta T = \Delta t_1 - \Delta t_2.$$

Based on the description above, ΔT represents the time difference between the average detected arrival time of photons and an expected arrival time of photons at an OM. The smaller the ΔT of the OM, the closer the angle of the photoelectrons collected within the OM to the Cherenkov emission angle.

Fig. 4 shows approximately 180 events, presented as a scatter plot of the time difference versus the median value of the real average photon emission angle from the track on the OM. The time difference is minimized at the Cherenkov angle. And consequently, the criteria for the time difference are in a range from 0 ns to 25 ns, as determined by the concentration of scattering at the 42° point.

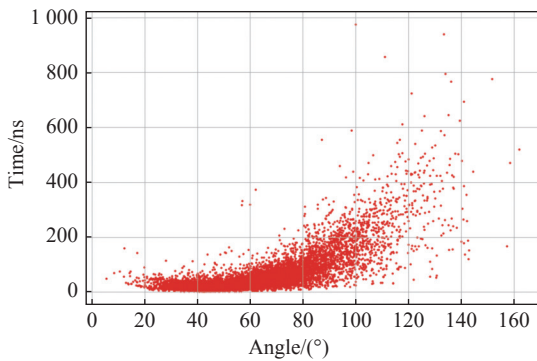


Fig. 4. The correlation between time difference and median value of the angle at which the photon leaves the track.

Following selection based on the time difference ΔT . In addition, the events used in reconstruction also need to pass another cut in which the ratio of the photons before and after the correction falls in a given range. This process enables the filtering out of OMs that are excessively large and erratic for reconstruction purposes, thereby

enhancing the precision of energy reconstructions. After optimization, the ratio range chosen for this selection is $[0, \mu \pm 2.3\sigma]$. μ and σ are the mean and RMS of ratio distribution. Fig. 5 illustrates the fraction of OMs filtered by time and ratio. In Fig. 5A, the percentage indicates the quantity of OMs discarded after the initial screening relative to the original number of OMs. The initial screening (time selection) results in the elimination of approximately 57% of OMs. In Fig. 5B, the percentage denotes the quantity of OMs discarded after the second round of screening in comparison to the number of OMs remaining after the first round. The OMs lost during the secondary screening (ratio selection) amounts to an additional 2.5%. In Fig. 5C, the quantity of OMs discarded after two rounds of screening as a proportion of the original number of OMs. In total, the two filters discarded roughly 58% of OMs in this scenario.

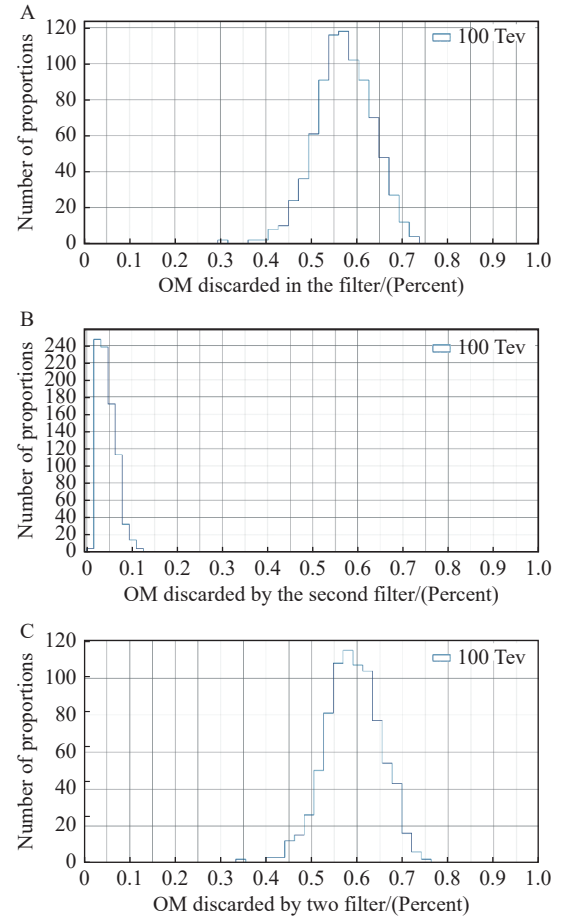


Fig. 5. Three graphs illustrating the percentage of OMs eliminated during the filtering process.

3.3. Photon Density Calculation

Due to the interactions caused by the movement of muons through water, a cascade is generated along the muon's track^[6], and we anticipate that the Cherenkov photons released within the cascade cluster will be integral to the energy reconstruction process. Consequently, the num-

ber of photons within the cluster is anticipated to vary with the track, enabling the reconstruction of photon density for different track lengths, which corresponds to the linear density of photons^[8, 9].

The photon density is calculated according to

$$\rho_{\text{ph}} = N_{\text{ph}}/\text{range}, \quad (4)$$

where N_{ph} is the total number of photons within a track length, denoted as *range*. The *range* is calculated starting from the array incident point of the pion. To obtain an optimal photon density, we calculate the density at various *ranges*.

Fig. 6A shows the mean of the photon density distribution at different ranges for all energies. It indicates that the separation of photon density between different energies is largest when the *range* is approximately 0–1700 m. The resolution of the energy reconstruction will be optimal at this photon density distribution.

Fixing the *range* parameter at 0–1700 m, the energy reconstruction curve can be derived by extracting the linear densities of photon numbers corresponding to the shaded regions in Fig. 6A^[10], giving the curve shown in

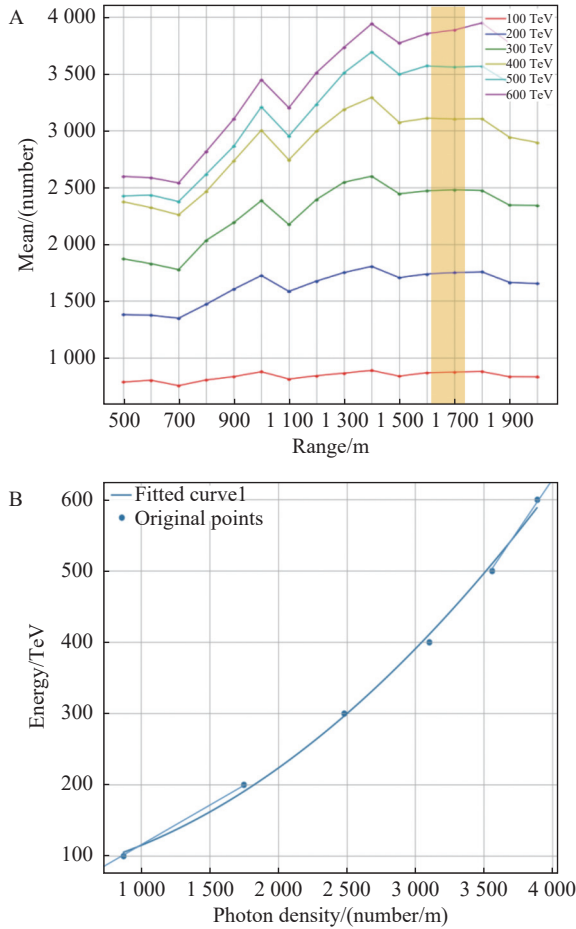


Fig. 6. A: Photon count density from the entry point to different ranges, from 500 m up to 2 000 m in 100 m increments. B: The energy reconstruction curve obtained within the 1 700 m range.

Fig. 6B, using the equation $y=0.00003x^2+0.01981x+65.20114$, where x is the photon density and y is the energy. The entire reconstructed curve is partitioned into three segments: the first segment is the line extending leftward between the first and second points on the curve; the second segment is the curve itself; and the third segment is the line extending rightward between the fifth and sixth points on the curve.

3.4. Results

To avoid fluctuations in photon density at different energies, we fit the curve in the below panel of Fig. 6 with a quadric curve of $y = 0.00003x^2 + 0.01981x + 65.20114$. The reconstructed errors of energy are shown in Fig. 7 using the parameter of $\log_{10}(E_{\text{re}} - E)$.

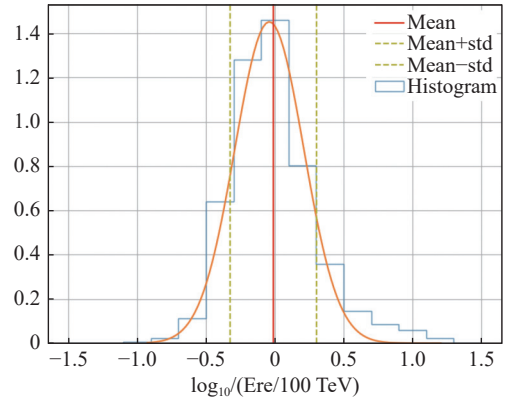


Fig. 7. The distribution of $\log_{10}(E_{\text{re}} - E)$ statistics for 100 TeV with standard deviation $\sigma=0.27$ is shifted to the left by 0.00997.

4. CONCLUSIONS

Here, we use two types of filters in the energy reconstruction process: temporal and ratio screening (see Section 3.2). Conventional energy reconstruction has a resolution of approximately 0.3. However, by employing the dual screening methods explained in this paper, we are able to increase the resolution of the 100 TeV energy reconstruction to 0.27, corresponding to an improvement of roughly 0.03. Through the relevant research in this paper, the gap of the HUNT project in neutrino energy reconstruction has been filled, and the accuracy of the HUNT project has initially reached that of other more complex experiments.

In future studies, we will optimize the detector simulation and reconstruction algorithms by taking further details (more diverse incident angle schemes; more complex algorithms, etc.) into account to further enhance the overall performance and accuracy of the reconstruction process. In the next phase of the experiment, we will deploy a prototype string into the optical array of Baikal-GVD and aim for improved results.

ACKNOWLEDGEMENTS

The work is supported by Institute of High Energy Physics (E25156U110), and the Sichuan Department of Science and Technology (2023YFSY0014).

AUTHOR CONTRIBUTIONS

Jiali Liu and Ying Qi proposed a method of energy reconstruction. Mingjun Chen was responsible for the management and supervision of the HUNT project. Zike Wang was responsible for the process of generating cases and the directional reconstruction of cases. Tianqi Huang and Peiyuan Chu were responsible for providing ideas and inspiration for the energy reconstruction method. Ying Qi was responsible for the programming and calculation of energy reconstructions. Jiali Liu, Maoyuan Liu and Ying Qi reviewed the manuscript. All authors read and approved the final manuscript.

DECLARATION OF INTERESTS

The authors declare no competing interests.

REFERENCES

- [1] Iyer Dutta, S., Reno, M. H., Sarcevic, I., et al. 2001. Propagation of muons and taus at high energies. *Physical Review D*, **63**(9): 094020.
- [2] Huang, T. Q., Cao, Z., Chen, M. J., et al. 2023. Proposal for the High Energy Neutrino Telescope. In Proceedings of the 38th International Cosmic Ray Conference (ICRC2023).
- [3] Abbasi, R., Abdou, Y., Ackermann, M., et al. 2013. An improved method for measuring muon energy using the truncated mean of dE/dx . *Nuclear Instruments and Methods in Physics Research Section A: Accelerators, Spectrometers, Detectors and Associated Equipment*, **703**: 190–198.
- [4] Agostinelli, S., Allison, J., Amako, K., et al. 2003. Geant4—a simulation toolkit. *Nuclear Instruments and Methods in Physics Research Section A: Accelerators, Spectrometers, Detectors and Associated Equipment*, **506**(3): 250–303.
- [5] Zornoza, J., Chirkin, D. 2007. Muon energy reconstruction and atmospheric neutrino spectrum unfolding with the IceCube detector. In Proceedings of the 30th International Cosmic Ray Conference. 5: 1275–1278.
- [6] Trovato, A., Drakopoulou, E., Sapienza, P. 2015. Muon track reconstruction and muon energy estimate in the KM3NeT/ARCA detector. In Proceedings of 34th International Cosmic Ray Conference.
- [7] Lundberg, J., Miočinović, P., Woschnagg, K., et al. 2007. Light tracking through ice and water—Scattering and absorption in heterogeneous media with Photonics. *Nuclear Instruments & Methods in Physics Research Section A: Accelerators, Spectrometers, Detectors and Associated Equipment*, **581**(3): 619–631.
- [8] Stettner, J., Michael, K., Wiebusch, C. 2021. Measurement of the energy spectrum of astrophysical muon-neutrinos with the IceCube Observatory. In Proceedings of the 40th International Conference on Environmental Systems.
- [9] Aartsen, M. G., Abbasi, R., Ackermann, et al. 2014. Energy reconstruction methods in the IceCube neutrino telescope. *Journal of Instrumentation*, **9**(3): P03009.
- [10] Schnabel, J. 2013. Muon energy reconstruction in the ANTARES detector. *Nuclear Instruments and Methods in Physics Research Section A: Accelerators, Spectrometers, Detectors and Associated Equipment*, **725**: 106–109.